

IPES: An Image Processing-Enabled Expert System for the Detection of Breast Malignant Tumors

¹R. M. Ghoniem, ²Basel Refky, ³Amr A. Soliman and ⁴Ahmed M. Tawfik

¹*School of Computer Science, University of Mansura, Mansura, Egypt;*

²*Department of Surgical Oncology, Oncology Center, University of Mansura, Mansura, Egypt;*

³*Universitätsklinik für Gynäkologie und Geburtshilfe, Klinikum Oldenburg, Fakultät für Medizin und Gesundheitswissenschaften, Universität, Oldenburg, Rahel-Straus-Straße 10, 26133 Oldenburg, Germany;*

⁴*Lecturer of Radiodiagnosis, Department of Diagnostic and Interventional Radiology, Mansura University Hospitals, Mansura School of Medicine, Egypt;*

prof_rania@mans.edu.eg; dr_basel@mans.edu.eg; amr.soliman@uni-oldenburg.de; ahm_m_tawfik@hotmail.com

ABSTRACT

Mammography is an influential screening tool for preliminary detection of breast carcinoma. However, interpreting mammograms is exhausting, particularly in the screening context. Moreover, sensitivity of mammography based screening is influenced by image quality and the experience level of radiologist. Thus, computer-aided diagnosis (CAD) programs can be utilized as a second-opinion tools that enhance the performance of radiologists, by consolidating sensitivity rates in contrast with those taken by double readings. The current paper is directed towards the integration of image processing and the rule-based reasoning into a diagnostic expert system for breast tumors. A proposed system termed *IPES* (Image Processing-enabled Expert System) is developed for the detection of breast malignant tumors, appear in mammography in three steps: (1) segmentation of mammographic masses from both pectoral muscle region and breast tissues, (2) Characterization of segmented masses upon the standards of Breast Imaging Reporting and Data System (BI-RADS) by: (i) shape-relevant features; (ii) margin characteristics; and (iii) density features, and (3) diagnosis of mass type upon some inference rules. The data set used for testing *IPES* contained 540 samples obtained from the standard Digital Database for Screening Mammography (DDSM). The Receiver Operator Characteristic (ROC) curves have been employed to evaluate the sensitivities and specificities of the system. Finally, the results reveal the efficacy of *IBES* in discriminating both malignant and benign breast masses.

Keywords: Image processing; expert systems; diagnosis of breast masses; mammography.

1 Background

Breast carcinoma is a diffuse cancer and the second leading reason for mortality among women [1]. Although variety of imaging tools such as Breast Thermography, Magnetic Resonance Imaging, Single Photon Emission Computed Tomography, Radiography, and Histopathology [2] have been employed as adjunct screening instruments for the high-risk women characterized by epidemiology-based risk

DOI: 10.14738/jbemi.36.2346

Publication Date: 2nd December 2016

URL: <http://dx.doi.org/10.14738/jbemi.36.2346>

models [3], mammography periodic screening is the most clinically accepted imaging modality for screening the general population to date [4].

Mammography interpretation is a labor-intensive job for radiology specialists, who cannot permanently supply steady consequences between readings. Moreover, the readings rely on the physician's training, expertise and subjective criteria [5, 6]. According to published statistics, about 10% of all malignant tumors in mammograms are missed by radiologists, and most of the missed tumors are in breasts of dense tissues [7]. Also, a high false positive rate is caused by mammography. Nearly 525 of 1800 lesions sent to biopsy are only malignant [8].

The causes of those high miss rates and low specificities of mammographic screenings involve: (1) the low conspicuity of mammogram lesions, (2) the image noisy nature which is a serious impeding factor that prohibits further reading of mammograms and (3) the overlying and underlying structures obscuring the image features [9, 10]. Moreover, the biopsies comprise minor hazards and are costly and extremely uncomfortable. To obviate dispensable biopsies, the false positive rate has to be minimized [5].

In this context, double reading of mammography (interpreting the same image by two radiologists) [11] was suggested to decrease the missed cancers rate. However, the workload and the expense accompanying double reading are high. Alternatively, CAD systems that include Expert systems (ESs) have evolved to help one individual radiologist when interpreting mammograms supplying support to his/her diagnosis. In addition, CAD systems can be employed as "second-opinion" criteria by radiologists, as they can play an efficient part in the preliminary detection of breast carcinoma in a cost-effective manner [12, 13].

ESs may be taken into consideration as a spin-off from artificial intelligence (AI) domain. The prevalent objective of AI is to capture and mimic both human decision-making and problem-solving processes, thus aiming to make computers deduce more like humans do. The three fundamental components of ES are usually distinguished as: a knowledge base (KB) of the domain related expertise, an inference engine for making deductions, and a user interface [14]. Consequently, recent advances in AI domain have led to the emergence of ESs for distinct medical applications. Furthermore, in the last few decades various intelligent tools have been designed to enhance the experiences and capabilities of physicians for making decisions concerned with patients.

In this context, different medical ESs that require a textual form for information input and output have been developed. Karabatak and Ince [15] presented an ES for diagnosing breast cancer using: (1) association rules, and (2) neural network. The ES diagnostic outputs were based on some required textual input information about number of breast cancer visual attributes, for instance, clump thickness, cell size uniformity, cell shape uniformity, marginal adhesion, and mitoses. The classification rate of the ES was 95.6%

Garibaldi et al [16] presented a fuzzy inference system for diagnosing breast cancer. The outputs of the system were recommendations of treatment upon assessment of five clinical variables: (1) Nottingham Prognostic Index (NPI), (2) estrogen receptor status, (3) invasion, (4) age, and (5) lymph node status. Results demonstrated that the model significantly raised performance to around 88.1%

Saraiva et al. [17] presented a hybrid approach for gastrointestinal cancer diagnosis based: (1) Case-Based Reasoning (CBR), and (2) Rule-Based Reasoning (RBR). A real patient data were used as inputs to the model while the output was the kind of gastrointestinal cancer. The results demonstrated that, with the presented approach, the diagnosis accuracy rose by 22.92% when compared with a CBR approach not employing RBR in case retrieval.

There are some observations on the previous studies: there are various medical domains that rely on expertise which is non-textual, such as radiology and oncology. Thus, the input information that normally present in non-textual form such as the visual attributes of cancer, has to be manipulated and transformed to textual form by the user. Consequently, the advices or results provided by the ES rely seriously on the efficiency with which the user can process and transform non-textual information. Formally speaking, the mapping from non-textual modes to text restricted forms is naturally liable to inconsistency, knowledge destruction, or knowledge damage.

Motivated by the need of an intelligent diagnostic tool for breast tumors that manipulates information in non-textual form, in this study, an image processing-enabled expert system termed *IPES* is designed to efficiently detect breast malignant tumors, appear in mammography in three main steps: (1) segmentation of mammographic masses from both pectoral muscle and breast tissues; (2) identification of segmented masses by: (i) shape-relevant features, (ii) margin characteristics and (iii) density features; and (3) diagnosis of mass type upon some inference rules.

2 Methodology

The parts of *IPES* architecture are shown in Figure 1 and detailed in the following subsections.

2.1 Segmentation of breast mass

Breast masses may appear in pectoral muscle or breast tissue. Therefore, an automatic segmentation method is proposed for accurately separating mammographic masses from pectoral muscle or breast tissues. The proposed method is described as:

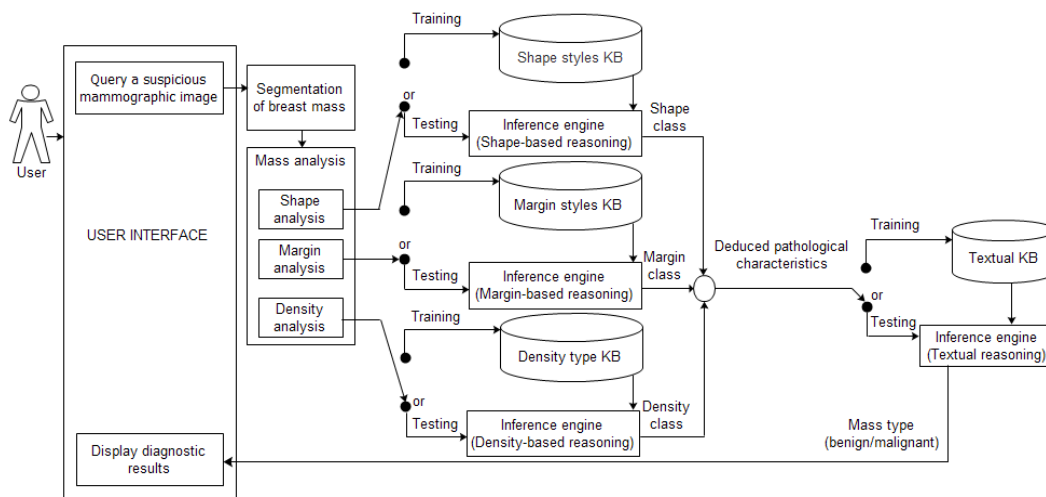


Figure 1: System architecture.

Step 1: Mammographic image enhancement

1. Apply the histogram equalization to greatly adjust mammograms intensities to enhance contrast.
2. Use the algorithm of median filtering for removing noise as follows:
 - a. Firstly, consider each pixel in mammogram in turn and inspect its adjacent neighborhood to determine if it can represent its surroundings.
 - b. Secondly, substitute the pixel value with the neighborhood pixel values median, where the median is obtained by first sorting all the surrounding neighboring pixels into numerical arrangement and then substituting the pixel being taken into account with the middle pixel value.

This step makes the brightness divergence between the mass and its surrounding tissue extremely apparent, simplifying the essential mass segmentation.

Step 2: Breast region extraction

The purpose of this step is to perfectly segment the breast region from the background of the image as follows.

1. A connected components labeling is employed as described further below:
 - a. The image is scanned and the underlying pixels are labeled in line with a predefined connectivity scheme and the relative values of their nearby neighbors. A 4-by-4 connected neighborhood is used to label the breast region object.
 - b. Morphological breast region opening and closing operations are then used with the aim of removing small artifacts in the image and smoothing the region contour.

Step 3: Pectoral muscle segmentation

For mammographic images, the region of pectoral muscle has a high density that leads to a strong margin approximated by a straight line. In this step, the region growing (RG) method and the morphological closing operation are used to extract the pectoral muscle from the breast region as follows.

1. For growing from the seed points, seed points and predetermined criteria are required for the step of RG.
 - a. Seed point selection: The RG begins with a number of the greatest pixel values pecked out from the pectoral muscle region to group adjoining pixels with homogeneous pixel values.
 - b. Region growing: Homogeneous pixels are iteratively collected until the RG rate goes beyond a predefined threshold t at this step. t is set as 0.5, taken from preliminary experiments, where different threshold values were used to test the selected data set. Consequently, the RG will be discontinued when the growing region area goes beyond 0.5 of the grouped region area. The resulting region is a breast pectoral muscle.
 - c. A morphological closing is then used to allocate a full contour of the pectoral muscle. This operation preserves the masses adjacent to the edge of this region.

Step 4: Mammographic mass segmentation

To initialize mass segmentation from pectoral muscle or breast tissues, two properties found in mammographic masses are used: (1) mass internal pixels are the brightest points in the mammograms; and (2) inner pixels display visually continuous variation. Thus, iterative thresholding followed by connectivity analysis are used in current step:

1. Suppose that s_j is the segmentation threshold. To pick out a new threshold, s_j is applied to each image to categorize pixels into one of two groups: mass or non-mass. Let μ_0 and μ_n be the gray level means of the two groups, respectively, after segmentation with s_j . Afterwards, the new threshold for $j+1$ step will become:

$$s_j = \frac{1}{2}(\mu_b + \mu_n) \quad (1)$$

where this iterative procedure goes on until the threshold is converged, moreover, the threshold computed for one mammogram cannot be considered for all images since the grey level variation of each mammogram is quite different, thus, the variation in grey levels is taken using histograms.

2. Perform the connectivity analysis of the thresholded images. The connected objects found in each breast or pectoral muscle image are counted and labeled. The largest components representing the breast and pectoral muscle masses are only detected.

Step 5: Reconstruction of mammographic mass margin

Because segmentation influences characterizing shapes and margins of masses, the morphological dilation is used for enhancing objects sizes. Consequently, the segmented masses will preserve both original shapes and marginal information. Eventually, the outcome of this step is intended to facilitate further mass analysis. The steps of tumor segmentation from both breast tissues and pectoral muscle are illustrated in Figures 2 and 3, respectively.

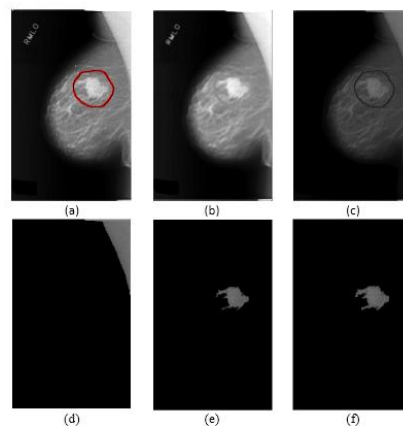


Figure 2: Steps of mass segmentation from breast tissue: (a) original mammographic image with a lobulated mass shape and microlobulated margin, (b) image enhancement, (c) breast region extraction, (d) pectoral muscle segmentation, (e) mass segmentation, and (f) reconstruction of mass margin.

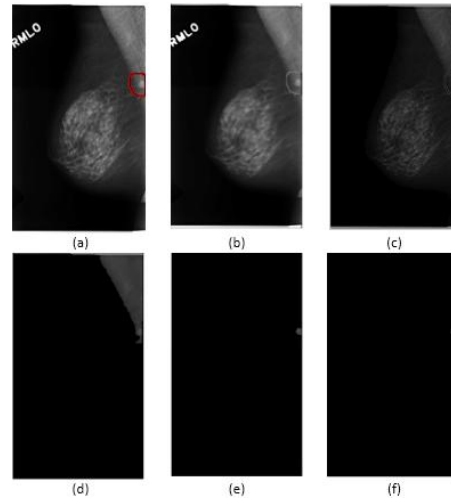


Figure 3: Steps of mass segmentation from pectoral muscle: (a) original mammographic image, (b) image enhancement, (c) breast region extraction, (d) pectoral muscle segmentation, (e) mass segmentation, and (f) reconstruction of mass margin.

2.2 Analysis of breast mass

Mammographic mass is characterized based on BI-RADS standards [18] by three characteristics are: (1) shape, (2) margin and (3) density, as demonstrated in Figure 4. These characteristics are utilized to decide if the mass is probably being benign or malignant.

2.2.1 Mass shape

Mass shape naturally implies an essential medical property. Zernike moments (ZMs) have been adduced to be an efficient descriptor for characterizing mass shape in [19]. Different Zernike polynomials (ZPs) and their corresponding physical meanings have been reported in [20]. In this paper, a combination of ZMs and five more geometric features are used to characterize the segmented mass shape.

For Cartesian coordinate system, computation of ZMs for a continuous image function $F(q, z)$ is given by Eq. 2 [21].

$$A_{ho} = \frac{h+1}{\pi} \iint_{q^2+z^2 \leq 1} F(q, z) V_{ho}^*(q, z) dqdz \quad (2)$$

where h and o denote order and repetition, respectively. The order h is a non-negative integer, the repetition o is an integer satisfying $h-|o| = \text{an even number}$ and $|o| \leq h$. V_{ho}^* refers to the Zernike basis function complex conjugate $V_{ho}(q, z)$ defined over the unit disk by [22]:

$$V_{ho}(q, z) = D_{ho}(P) e^{io\theta} \quad (3)$$

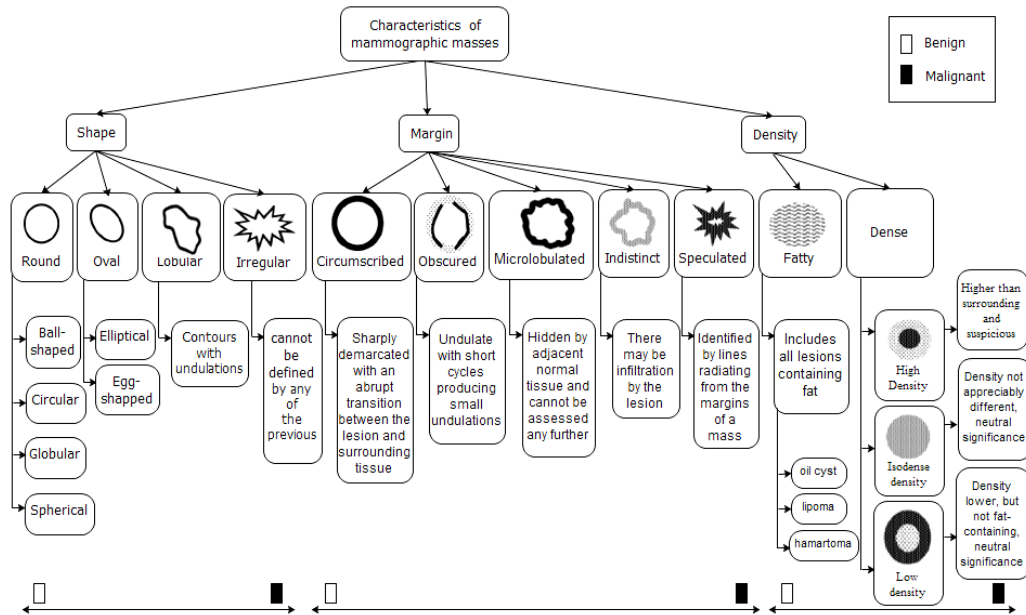


Figure 4: Characteristics of mammographic masses used in this paper based BI-RADS standards.

$$P = \sqrt{q^2 + z^2}, (P \leq 1), \theta = \tan^{-1} \left(\frac{q}{z} \right) \quad (4)$$

where l is the imaginary unit $\sqrt{-1}$. Radial Zernike polynomial D_{ho} is calculated using Eq. 5 [23].

$$D_{ho}(P) = \frac{h - |o|}{2} \sum_{l=0}^{h-|o|} \frac{(-1)^l (P)^{h-2l} (h-l)!}{l! \left(\frac{h+|l|}{2} - l \right)! \left(\frac{h-|l|}{2} - l \right)!} \quad (5)$$

Since the ZMs represent the projection of image $F(q, z)$ onto those orthogonal basis functions, the image I_0 can be divided into a weighted sum of ZPs using Eq. 6 [24]:

$$F(q, z) = \sum_{h=1}^{\infty} \sum_{o=-h}^h A_{ho} V_{ho}, \quad (6)$$

where $I_{h,o}$ indicates the ZMs, that constitute the coefficients of the ZPs.

The first 4-order ZMs (produce a total of 15 ZMs), extracted in this paper, and five more features that measure the geometric attributes of the segmented masse are combined to obtain a robust final feature vector (Table 1). The selected geometric features are illustrated as follows:

- Area: The area specifies the size of the mammographic mass, which is expressed using Eq. 22, where R indicates the set of pixels points inside the mass.
- Perimeter: Suppose that s_1, \dots, s_N denote the pixels locations on the mass contour. Mathematically, the perimeter feature represents the sum of distances between neighboring pixels, which is calculated using Eq. 23.

Table 1. The Zernike polynomials and geometric features used to characterize mass shape.

Descriptor	Equation
Piston	$A_{0,0} = -1$ (7)
distortion (x direction)	$A_{1,-1} = -2P \sin \theta$ (8)
distortion (y direction)	$A_{1,1} = 2P \cos \theta$ (9)
Astigmatism ($\pm 45^\circ$)	$A_{2,-2} = \sqrt{6} P^2 \sin 2\theta$ (10)
Spherical defocus	$A_{2,0} = \sqrt{3}(2P^2 - 1)$ (11)
Astigmatism (0° or $\pm 90^\circ$)	$A_{2,2} = \sqrt{6} P^2 \cos 2\theta$ (12)
Triangular astigmatism (x - axis)	$Z_{3,-3} = \sqrt{8} P^3 \sin 3\theta$ (13)
Coma (along x - axis)	$A_{3,-1} = \sqrt{8}(3P^3 - 2P) \sin \theta$ (14)
Coma (along y - axis)	$A_{3,1} = \sqrt{8}(3P^3 - 2P) \cos \theta$ (15)
Triangular astigmatism (y - axis)	$A_{3,3} = \sqrt{8} P^3 \cos 3\theta$ (16)
Quatrefoil	$A_{4,-4} = \sqrt{10} P^4 \sin 4\theta$ (17)
Astigmatism (5-order)	$A_{4,-2} = \sqrt{10}(4P^4 - 3P^2) \sin 2\theta$ (18)
Spherical aberration	$A_{4,0} = \sqrt{5}(6P^4 - 6P^2 + 1)$ (19)
Astigmatism (5-order)	$A_{4,2} = \sqrt{10}(4P^4 - 3P^2) \cos 2\theta$ (20)
Quatrefoil	$A_{4,4} = \sqrt{10} P^4 \cos 4\theta$ (21)
Area	$A = \pi $ (22)
Perimeter	$P = \sum_{i=1}^{N-1} x_i - x_{i+1} $ (23)
Compactness	$C = \frac{P^2}{4\pi A}$ (24)
Circularity	$L = \frac{4\pi d}{(r_{convex})^2}$ (25)
Eccentricity	$M_{11} = \sum_{n=1}^N (a_n - A_0), M_{22} = \sum_{n=1}^N (b_n - B_0)^2$ $M_{12} = M_{21} = \sum_{n=1}^N (a_n - A_0)(b_n - B_0)$ (26)
	$r_1 = \sqrt{\frac{\lambda_1}{2}}, r_2 = \sqrt{\frac{\lambda_2}{2}}$ (27)
	$E = \frac{r_1}{r_2}$ (28)

^a θ is the angle with y axis

- Compactness: Describes the contour complexity versus enclosed region, where P and A are the mass perimeter and area respectively, as demonstrated in Eq. 24.
- Circularity: The circularity C indicates how circular a certain mass is and is defined using Eq. 25, where P is the convex hull perimeter.
- Eccentricity: Is a measure of the mass lengthiness as illustrated in Eq. 26, where E is a symmetric matrix, N is the mass pixels number, (x, y) point out to the generic pixel coordinates, (x_c, y_c) indicate the mass geometric center coordinates. If λ_1 and λ_2 represent the eigenvalue of E , in the mass region elliptical approximation, the semi-axis values will be determined using Eq. 27, the eccentricity is then calculated using Eq. 28. Values close to 1 refer to circular masses, whereas values close to zero indicate more stretched masses.

2.2.2 Mass margin

In this paper, the steps of extracting the mass margin features are described as:

- Step 1: Segment the outer boundary of the mass object using Canny edge detector.
- Step 2: Reduce the width of the mass boundary to one pixel using the edge detector of Susan thinning [25]. For each segmented mass, the pixel is measured and considered border pixel if any one of its neighboring pixels is white. Initially, all the pixels are considered as border chains. Afterwards, the pixels for each chain are eliminated in such a way that these eliminated pixels do not affect the border connectedness. After all, a mass with one-pixel contour is produced.
- Step 3: Segment the inner shape of the mass object using the erosion morphological operation to reduce the object size.
- Step 4: Compute the mass variation and sharpness degrees [26] according to Eq. 29

$$v = \frac{c_{outer}}{a_{inner}},$$

$$s = \frac{b_{outer}}{b_{inner}}, \quad (29)$$

where v is the mass variation degree, s is the mass sharpness degree, c_{outer} is the number of light pixels points in the mass outer border, a_{inner} is the area of the mass inner shape, b_{outer} is the variation in the outer boundary's brightness and b_{inner} is the variation in the inner shape's brightness.

2.2.3 Mass density

This paper presents proposed method for mass density characterization by grouping the pixels inside the mass according to their appearance, as follows:

- Step 1: Compute the Wavelet packet transform of an $R \times B$ discrete image Z of a segmented tumor up to level $L+1$ ($L \leq \min(\log_2 R, \log_2 B)$), where the image is actually decomposed into 1-approximation and 3-detail images, using two filters are low-pass H and high-pass G , then the resulted image are decomposed into a second-level approximated and detailed images, furthermore, the process is repeatedly implemented until the third level, as follows:

$$E_{4c,(s,u)}^{l+1} = \sum_m \sum_n H(b)G(r) E_{c,(b+2s,r+2u)}^l, \quad (30)$$

$$E_{4c+1,(s,u)}^{l+1} = \sum_m \sum_n H(b)G(r) E_{c,(b+2s,r+2u)}^l, \quad (31)$$

$$E_{4c+2,(s,u)}^{l+1} = \sum_m \sum_n H(b)G(r) E_{c,(b+2s,r+2u)}^l, \quad (32)$$

$$E_{4c+3,(s,u)}^{l+1} = \sum_m \sum_n H(b)G(r) E_{c,(b+2s,r+2u)}^l, \quad (33)$$

where $E_{0,(s,u)}^0$ is the image Z . At each stage, the image E_c^l is divided into four quarter-size images E_{4c}^{l+1} , E_{4c+1}^{l+1} , E_{4c+2}^{l+1} , E_{4c+3}^{l+1} , further, the Daubechies wavelet of order 8 (db8) is used to implement this computing.

- Step 2: Broke each terminal node of the decomposition tree into k windows/regions of 3×3 neighborhood. For each region, a center-symmetric local binary patterns (CS-LBP) is computed as follows:

$$CSLBP_{D,Y,S}(a,b) = \sum_{c=0}^{(Y/2)-1} s(y_c - y_{c+(Y/2)}) 2^c, \quad h(a) = \begin{cases} 1, & a > S, \\ 0 & \text{otherwise} \end{cases}, \quad [24] \quad (34)$$

where y_c and $y_{c+(Y/2)}$ are the intense values of the center-symmetric pairs of points of Y equally distanced pixels on a radius circle D , S is the value employed to threshold the gray-level differences, whereas, experiments showed that 8, 1, 0.02 are efficient values for the parameters Y , D , and S , respectively.

- Step 3: Concatenate the CS-LBP based features corresponding to the k neighborhood regions of the terminal nodes, to form the final descriptor that characterizes the tissue appearance of the mass.
- Step 4: Group the pixels inside the mass according to their appearance using the fuzzy c-means (FCM). The result of this step is the division of the mass into two separate categories: (1) fatty tissue and (2) dense tissue. The FCM aims to find fuzzy partitioning for the given mass descriptor through minimization of the objective functional as follows:

$$J_i(Q;V;Z) = \sum_{e=1}^f \sum_{g=1}^n (\mu_{eg})^i D_{eg}, \quad (35)$$

where $Q=[q_1, q_2, \dots, q_n]$ represents a set of n local patterns, q_g is the g th pattern $\in Q$, $V=[\mu_{eg}] \in I_{fcn}$ is the matrix of fuzzy partition of Q , $Z=[z_1, z_2, \dots, z_f]$ contains f number of cluster prototypes vectors $z_e=(z_e, 1 \leq e \leq f)$, $D_{eg} = \left\| \begin{matrix} Q \\ g \end{matrix} - Z_e \right\|^2$ (Euclidean norm) indicates the dissimilarity measure among the sample q_g and each cluster center, further, the cluster center is computed using

$$Z_e = \frac{\sum_{g=1}^n (\mu_{eg})^i q_g}{\sum_{g=1}^n (\mu_{eg})}, \quad (36)$$

where μ_{eg} is the grade of belonging of a pattern q_g to each cluster, that is defined as

$$\mu_{eg} = \frac{1}{\sum_{j=1}^f \left(\frac{d_{eg}}{d_{jg}} \right)^{\frac{2}{i-1}}}, \quad (37)$$

where i and f is a parameter, which controls the algorithm fuzziness. Moreover, the following two constraints have to be achieved during optimization of the functional : (1) and (2).

- Step 5: Extract the mean statistic from all clusters in order to describe both fatty and dense regions, which are related to the clusters morphology. Furthermore, the grey level mean of each cluster is then employed to accomplish a ranking of cluster densities: a higher mean correlates with a higher likelihood of being a cluster with a dense tissue.
- Step 6: Use the resulting vector of clusters densities ranking to train density type KB.

2.3 Knowledge bases construction

In terms of ESs, the knowledge acquired from knowledge source is represented in KB by production rules of the form:

$$\text{IF} \langle \text{given} - \text{condition} \rangle \text{ THEN} \langle \text{resulted} - \text{conclusion} \rangle$$

Thus, the knowledge extracted from segmented masses about their shapes, margins, and densities is respectively stored in the shape style KB, margin style KB, and the density type KB. An example of some production rules that describe mass shape analysis is provided in Figure 5.

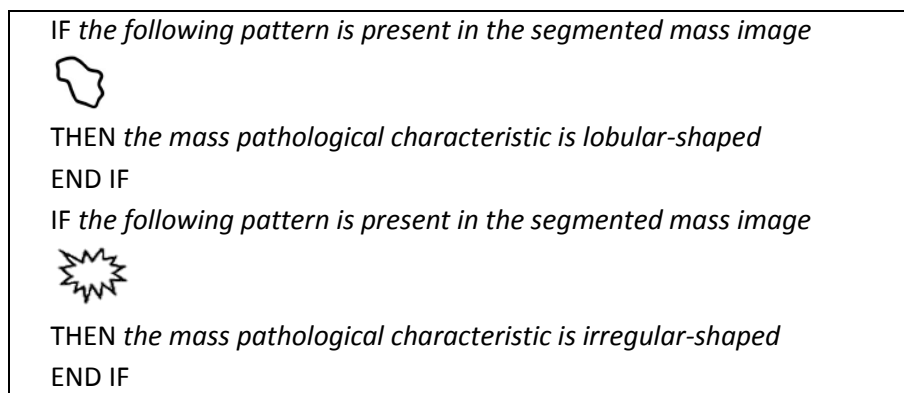


Figure 5: Some sample production rules in IPES shape style KB.

Therefore, the fact bases of shape style, margin style, and the density type include the data taken by mass analysis algorithms. Inferred knowledge is dynamically inserted through the inferring processes. Likewise, rules are used to accomplish the characterization of the objects to be classified. In other words, the rules relate the parameters taken by mass analysis algorithms to the diagnosis. Besides, they operate on different criteria as the object morphologic characteristics, the occurrence of particular patterns in the analyzed mass, or comparing any object under detection with other reference objects.

Furthermore, the textual knowledge acquired from BI-RADS about different combinations of mass shapes, margins, densities, was respectively represented in a corresponding KB. For instance, the interaction of shape and margin characteristics with each other through the mass development course may have various likelihood degrees of benignancy or malignancy. Round, oval and lobular-shaped masses have an obvious smooth edges which are commonly diagnosed as benign signs, nevertheless they are still potentially to be malignant if their margins are not smooth. Also, irregular-shaped masses predominantly appear with indistinct or speculated margins, which are significant evidences of malignancy. An example of some production rules that represent the combinations of the mass three pathological characteristics in the textual KB is presented in Figure 6. The outline of KBs in this paper was defined by CLIPS commands. Figure 7 demonstrates the representation of some rules in the textual KB using CLIPS.

2.4 Inference engines development

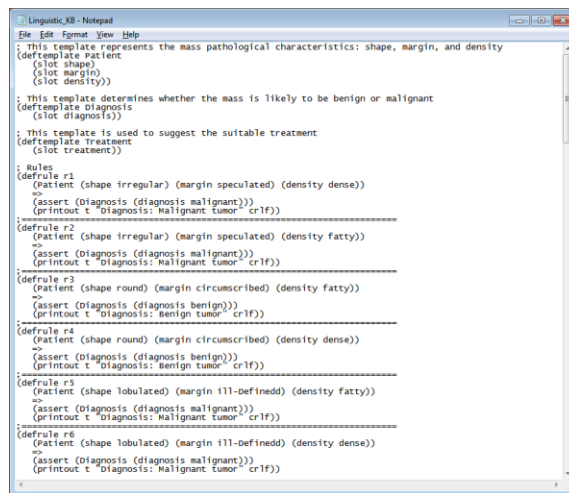
This stage involves the adoption of an inference strategy for the task of rule analysis. *IPES* uses the forward chaining (data-driven reasoning) as its inference mechanism. Thus the chaining begins with known data and proceeds toward a conclusion. In testing phase, the query image is matched with the shape style, margin style, and density type KBs, respectively, using the corresponding inference engines. Afterwards, *IPES* takes the inference results obtained from those matching processes to perform a final reasoning operation on the information stored in the textual KB, in order to reach appropriate conclusion about the mass likelihood degree of being benign or malignant.

2.5 User interface

Image of a suspicious mammogram can be immediately read and interpreted through *IPES* user interface. Once a suspicious image is selected, the mammographic mass is segmented, analyzed and diagnosed. Consequently, *IPES* interactively displays the diagnosis results which involve the shape style, margin style, density type, pathology type, the region that mass appears within, and number of abnormalities.

```
IF the mass is irregular-shaped
AND
The mass margin is speculated
AND
The mass density is dense
THEN
The diagnosis indicates malignant tumor
END IF
IF the mass is lobular-shaped
AND
The mass margin is circumscribed
AND
The mass density is fatty
THEN
The diagnosis indicates benign tumor
END IF
```

Figure 6: Some sample production rules in *IPES* textual KB.



```
Linguistic_KB - Notepad
File Edit Format View Help
: This template represents the mass pathological characteristics: shape, margin, and density
(deftemplate Patient
  (slot shape)
  (slot margin)
  (slot density))
: This template determines whether the mass is likely to be benign or malignant
(deftemplate Diagnosis
  (slot diagnosis))
: This template is used to suggest the suitable treatment
(deftemplate Treatment
  (slot treatment))
: Rules
(defrule r1
  (Patient (shape irregular) (margin speculated) (density dense))
  =>
  (assert (diagnosis (diagnosis malignant)))
  (printout t "diagnosis: malignant tumor" crlf))
-----
(defrule r2
  (Patient (shape irregular) (margin speculated) (density fatty))
  =>
  (assert (diagnosis (diagnosis malignant)))
  (printout t "diagnosis: malignant tumor" crlf))
-----
(defrule r3
  (Patient (shape round) (margin circumscribed) (density fatty))
  =>
  (assert (diagnosis (diagnosis benign)))
  (printout t "diagnosis: benign tumor" crlf))
-----
(defrule r4
  (Patient (shape round) (margin circumscribed) (density dense))
  =>
  (assert (diagnosis (diagnosis benign)))
  (printout t "diagnosis: benign tumor" crlf))
-----
(defrule r5
  (Patient (shape lobulated) (margin ill-defined) (density fatty))
  =>
  (assert (diagnosis (diagnosis malignant)))
  (printout t "diagnosis: malignant tumor" crlf))
-----
(defrule r6
  (Patient (shape lobulated) (margin ill-defined) (density dense))
  =>
  (assert (diagnosis (diagnosis malignant)))
  (printout t "diagnosis: malignant tumor" crlf))
```

Figure 7: Some production rules with CLIPS that represent the combinations of the mass three pathological characteristics in the textual KB.

3 Experimental Results

3.1 Database

The mammograms used in this study were taken from the standard DDSM [25]. This database contains 2620 cases, organized in 43 volumes. Furthermore, the case of one patient is a set of mammograms corresponding to one mammography population. The database presents chain codes of the suspected regions and each abnormality metadata according to BI-RADS standards.

The data set selected for testing *IPES* contained 540 samples. Table 2 illustrates the classes of pathological characteristics, the class number and percentage of images. These classes were chosen according to two criteria: (1) available image amount, (2) existence of pathological characteristics used for testing, and (3) exclusion of images that do not contain pectoral muscle.

Table 2. The ground truth of mammographic masses used to evaluate *IPES* performance

Mass type	Shape style	Margin style	Sample numbers		Proportion
			Fatty	Dense	
Malignant	Irregular	Speculated	65	40	19.4%
	Irregular	Ill-Defined	19	67	15.9%
	Lobulated	Ill-Defined	16	10	4.8%
	Lobulated	Micro lobulated	10	5	2.8%
	Round	Ill-Defined	5	5	1.9%
	Irregular	Micro lobulated	8	1	1.7%
	Oval	Speculated	5	2	1.3%
	Lobulated	Speculated	5	2	1.3%
Benign	Round	Speculated	4	2	1.1%
	Oval	Circumscribed	42	18	11.1%
	Oval	Obscured	24	27	9.4%
	Lobulated	Circumscribed	36	11	8.7%
	Oval	Ill-Defined	16	10	4.8%
	Round	Circumscribed	10	12	4.1%
	Lobulated	Obscured	20	22	7.8%
Round	Obscured	9	12	3.9%	
Total			246	294	100%

3.2 Evaluation criteria

The performance of *IPES* was evaluated by comparing its outputs to the diagnostic information provided by DDSM and realized by the authors. The performance of each reasoning test was characterized in terms of the capability of the system to differentiate true positives while declining false positives. The following two equations were used to compute the rates of both true positive and false positive, indicated by TPR and FPR, respectively.

$$TPR = \frac{TPN}{FNN + TPN} \tag{38}$$

$$FPR = \frac{FPN}{TNN + FPN} \tag{39}$$

where the number of the true positive, false negative, false positive, and true negative test results, indicated by TPN, FNN, FPN, and TNN respectively. On the other hand, the sensitivity and specificity measures were also used, which are defined by Eqs. 40 and 41, respectively:

$$\text{Sensitivity (ST)} = TPR = \frac{TPN}{FNN + TPN} \tag{40}$$

$$\text{Specificity (SF)} = 1 - FPR = \frac{TNN}{TNN + FPN} \tag{41}$$

Furthermore, the ROC curves were used to illustrate the connection between both TPR (sensitivity) and FPR (1-specificity) across all potential cutoff values that depict the test positivity. The area under curve (AUC) demonstrates a measure of the classifier discrimination capability across a whole range of cutoffs [26].

3.3 Protocol

IPES operates in two fundamental steps: (1) training, and (2) testing. The "leave-one-out" method was employed to test the system performance. The images were divided into 10 groups, each time nine groups were taken for *IPES* training and the rest (leave-one-out) for the reasoning test.

3.4 Discussion

For the shape-based reasoning, four distinct shape classes indicated by round (59), oval (144), lobulated (137), and irregular (200), were used. Figure 8a presents the ROC curve obtained with this reasoning test ($AUC=0.981$, $SE=98.7$, $SP=100\%$). Reasoning results verify the efficiency of the shape analysis method for discriminating both regular and irregular-shaped masses.

Five classes of margins, including: ill-defined (148), speculated (125), obscured (114), circumscribed (129), and microlobulated (24), were used for margin-based reasoning. Figure 8b presents the ROC curve obtained with the proposed margin feature extraction method ($AUC=0.982$, $ST=98.5$, $SF=100\%$). The results indicate that masses with circumscribed and microlobulated margins can be effectively discriminated rather than the other three types.

Two types of breast tissue, including: fatty (246) and dense (294), were used for density-based reasoning. Figure 8c illustrates the ROC curve obtained with the proposed density analysis method ($AUC=0.979$, $ST=98.4$, $SF=100\%$). Reasoning results reveal that, this method is efficient for both fatty and dense mammographic masses.

Finally, after the tested images are matched with the shape style, margin style, and density type KBs respectively using the corresponding inference engines, the inference results are obtained to perform the final reasoning on the information stored in the textual KB. The result of this test provides appropriate conclusion about the mass likelihood degree of being benign or malignant. Figure 8d shows the ROC curve obtained with the textual reasoning ($AUC=0.976$, $ST=98.1$, $SF=100\%$). Results indicate the effectiveness of *IPES* in discriminating malignant and benign breast masses.

4 Conclusions

The main objective of this paper was to integrate both image processing and the rule-based reasoning into a diagnostic expert system for breast tumors. An image processing-enabled expert system termed *IPES* was presented for the detection of breast benign and malignant masses. First of all, an automatic segmentation method has been proposed for segmenting mammographic masses from pectoral muscle and breast tissue. After segmentation, mammographic masses were identified and mainly described based on the standards of BI-RADS by: (1) shape-relevant features, (2) margin characteristics, and (3) density type. The knowledge extracted from segmented masses about their shapes, margins, and densities is respectively stored in the shape style KB, margin style KB, and the density type KB. Furthermore, the textual knowledge acquired from BI-RADS about different combinations of mass shapes, margins, densities, was respectively represented in a corresponding KB. In testing phase, the query image is matched with the shape style KB, margin style KB, and density type KB, respectively, using the corresponding inference engines. Afterwards, *IPES* takes the inference results obtained from those matching processes to perform a final reasoning operation on the information stored in the textual KB, in order to reach appropriate conclusion about the mass likelihood degree of being benign or

malignant. ROC curves were used to compare sensitivities and specificities of each reasoning test. The empirical conclusions of the research showed that ST for the four reasoning tests were 98.7%, 97.5%, 97.4% and 98.1%, respectively, while the obtained SF of each test was 100%. Results indicate the effectiveness of *IPES* in discriminating the malignant and benign breast masses.

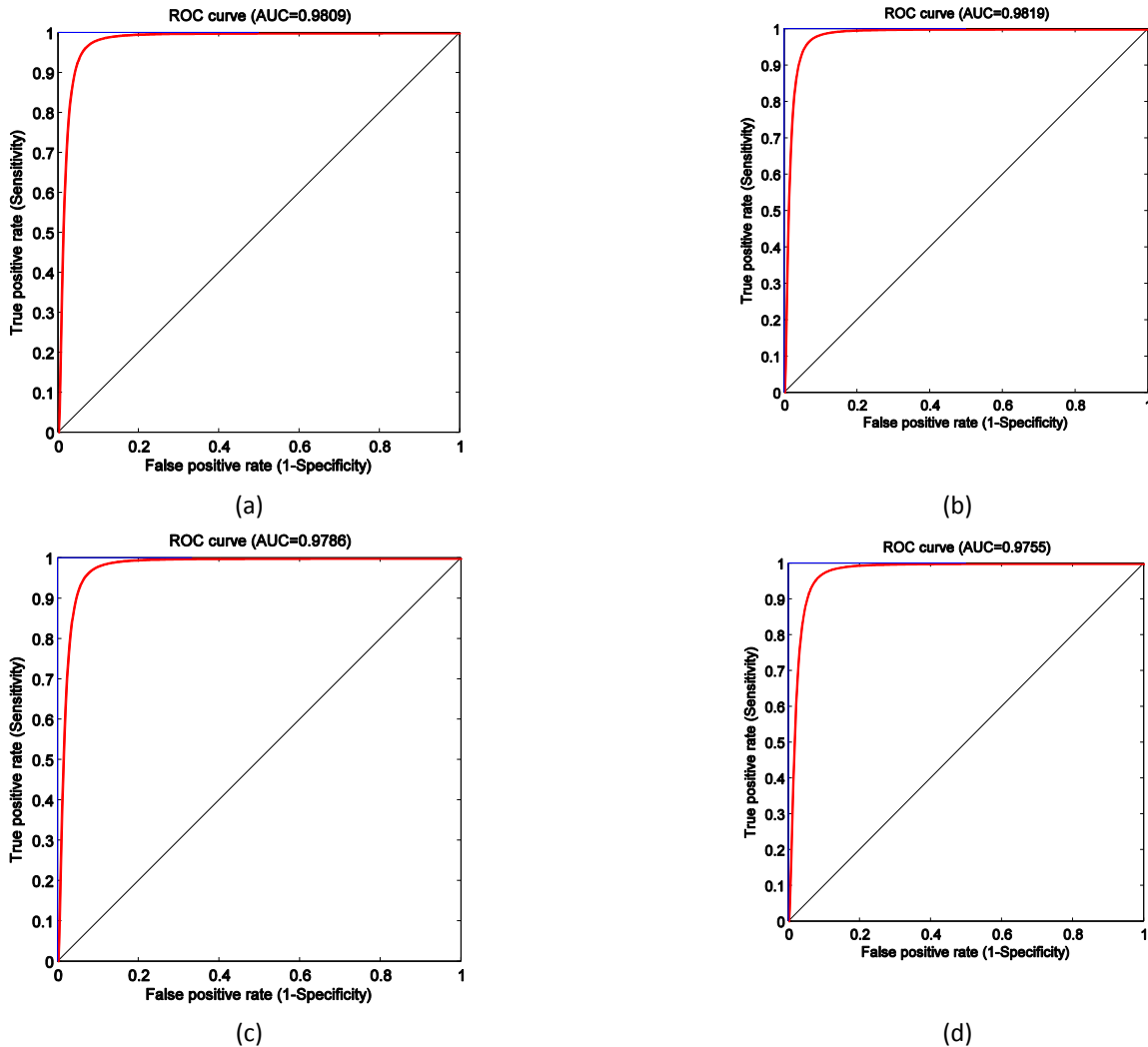


Figure 8: ROC curves obtained for (a) shape-based reasoning (AUC=0.981, SE =98.7 , SP=100%), (b) margin based-reasoning (AUC=0.982, SE =98.5, SP=100%), (c) density-based reasoning (AUC=0.979, SE =98.4, SP=100%), and (d) textual reasoning (AUC=0.976, SE =98.1, SP=100%).

APPENDIX

CLIPS programming language was used to construct KBs and develop inference engines of *IPES*. MATLAB was used to build image processing algorithms and user interface of the system. The main interface of *IPES* is shown in Figure 9, which assist user to process and diagnose the selected mammogram. A Snapshot of mass segmentation is presented in Figure 10. Figure 11 demonstrates a snapshot of the mass density analysis. The multi-resolution analysis of the segmented mass is shown in Figure 12. The interface of mass margin analysis is shown in Figure 13, which help user to extract and study the segmented mass margin. Figure 14 shows a snapshot of the final case report provided by *IPES*

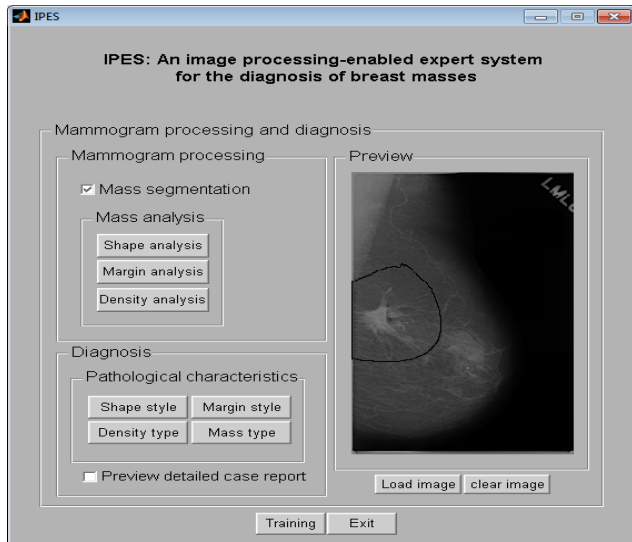


Figure 9: Snapshot of the main interface of *IPES*



Figure 10: Snapshot of mass segmentation

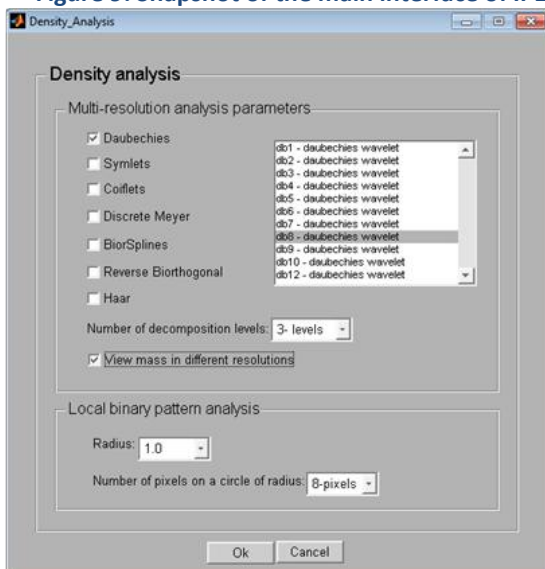


Figure 11: Snapshot of mass density analysis.

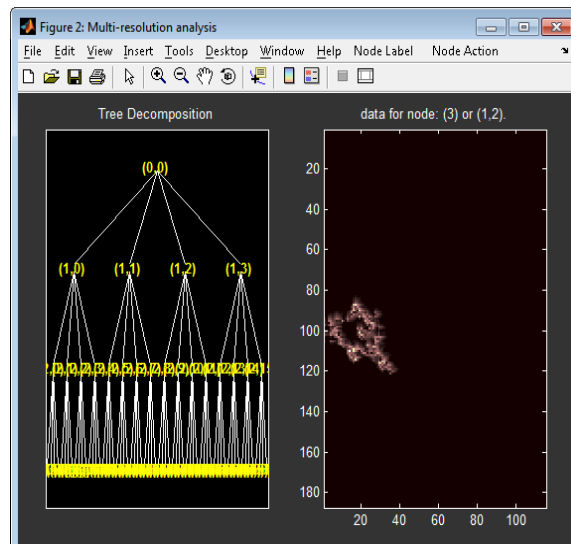


Figure 12: Snapshot of the multi-resolution analysis of the segmented mammographic mass

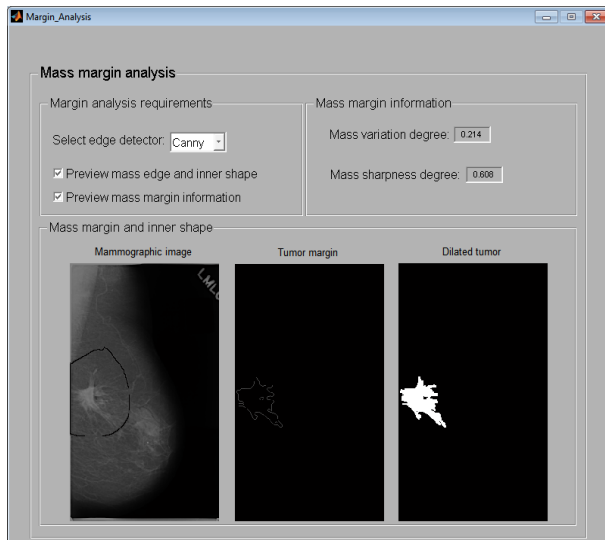


Figure 13: Snapshot of mass margin analysis

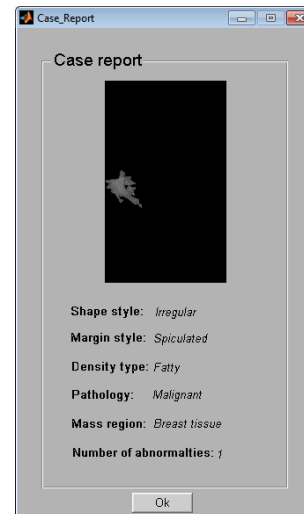


Figure 14: Snapshot of the final case report provided by IPES

REFERENCES

- [1]. Niwas, S.I., Palanisamy, P., Chibbar, R., Zhang, W., An expert support system for breast cancer diagnosis using color wavelet features. *J Med Syst.*, 2012. 36(5): p. 3091-3102.
- [2]. Hayat, M. A., *Cancer imaging: lung and breast carcinomas*, 2008, Elsevier Academic Press: USA.
- [3]. Amir, E., Freedman, O.C., Seruga, B., Evans, D.G., Assessing women at high risk of breast cancer: a review of risk assessment models. *J Natl Cancer Inst.*, 2010. 102(10): p. 680–691.
- [4]. Wang, X., Li, L., Liu, W., Xu, W., Lederman, D., Zheng, B., An interactive system for computer-aided diagnosis of breast masses. *J Digit Imaging*, 2012. 25(5): p. 570–579.
- [5]. Shi, X., Cheng, H.D., Hu, L., Ju, W., Tian, J., Detection and classification of masses in breast ultrasound images. *Digit Signal Process.*, 2010. 20(3): p. 824-836.
- [6]. L. de Oliveira Martins, Silva, A.C., A.C. de Paiva, Gattass, M., Detection of breast masses in mammogram images using growing neural gas algorithm and Ripley's K function. *J Sign Process Syst.*, 2009. 55(1): p. 77–90.
- [7]. Jackson, V., Hendrick, R., Feig, S., Kopans, D., Imaging of the radiographically dense breast. *Radiology*, 1993. 188(2): p. 297–301.
- [8]. Dennis, M.A., Parker, S.H., Klaus, A.J., Stavros, A.T., Kaske, T., Clark, S.B., Breast biopsy avoidance: The value of normal mammograms and normal sonograms in the setting of a palpable lump. *Radiology*, 2001. 219(1): p. 186–191.
- [9]. Sivaramakrishna, R., Powell, K.A., Lieber, M.L., Chilcote, W.A., Shekhar, R., Texture analysis of lesions in breast ultrasound images. *Comput. Med. Imaging Graph.*, 2002. 26(5): p. 303–307.
- [10]. Buist, D.S., Anderson, M.L., Haneuse, S.J., Sickles, E.A., Smith, R.A., Carney, P.A., Taplin, S.H., Rosenberg, R.D., Geller, B.M., Onega, T.L., Monsees, B.S., Bassett, L.W., Yankaskas, B.C., Elmore, J.G., Kerlikowske, K., Miglioretti, D.L., Influence of annual interpretive volume on screening mammography performance in the United States. *Radiology*, 2011. 259(1): p. 72–84.

- [11]. Brown, J., Bryan, S., Warren, R., Mammography screening: An incremental cost effectiveness analysis of double versus single reading of mammograms. *BMJ*, 1996. 312(7034): p. 809–812.
- [12]. Ramos-Pollán, R., Guevara-López, M.A., Suárez-Ortega, Díaz-Herrero, G., Franco-Valiente, J.M., Rubio-Del-Solar, M., González-de-Posada, N., Vaz, M.A., Loureiro, J., Ramos, I., Discovering mammography-based machine learning classifiers for breast cancer diagnosis. *J Med Syst.*, 2012. 36(4): p. 2259-2269.
- [13]. Markey, M.K., Bovik. A.C., Computer-Aided Detection and Diagnosis in Mammography, in *Handbook of Image and Video Processing*, A.C. Bovik, Editor 2005, New York: Academic, p. 1195-1217.
- [14]. Dhaliwal, J.S., Benbasat, I., The Use and Effects of Knowledge-Based System Explanations: Theoretical Foundations and a Framework for Empirical Evaluation. *Information Systems Research*, 1996. 7(3): p. 342-366.
- [15]. Karabatak, M., Cevdet Ince, M., An expert system for detection of breast cancer based on association rules and neural network. *Expert Systems with Applications*, 2009. 36(2): p. 3465–3469.
- [16]. Garibaldi J.M., et al., Incorporation of expert variability into breast cancer treatment recommendation in designing clinical protocol guided fuzzy rule system models. *Journal of Biomedical Informatics*, 2012. 45(3): p. 447–459.
- [17]. Saraiva, R., et al., Early diagnosis of gastrointestinal cancer by using case-based and rule-based reasoning. *Expert Systems with Applications*, 2016. 61(1): p. 192–202.
- [18]. American College of Radiology, *The ACR Breast Imaging Reporting and Data System (BI-RADS)*, 4th ed., American College of Radiology, Reston,VA, 2003.
- [19]. Wei, C.-H., Chen, S.Y., Liu, X., Mammogram retrieval on similar mass lesions. *Computer Methods and Programs in Biomedicine*, 2012. 106(3): p. 234–248.
- [20]. Zhu, L., Sun, P.-C., Bartsch, D.-U., Freeman, W.R., Fainman, Y., Wave-front generation of Zernike polynomial modes with a micromachined membrane deformable mirror for Optical Metrology. *Applied Optics*, 1999. 38(28): p. 6019-6026.
- [21]. Walia, E., Goyal, A., Brar, Y.S., Zernike moments and LDP weighted patches for content based image retrieval. *Signal, Image and Video Processing*, 2014. 8(3): p. 577-594.
- [22]. Goyal, A., Walia, E., Variants of dense descriptors and Zernike moments as features for accurate shape-based image retrieval. *Signal, Image and Video Processing*, 2014. 8(7): p. 1273-1289.
- [23]. Yang, M., Kpalma, K., Ronsin, J., Shape-based invariant feature extraction for object recognition, In *Advances in Reasoning-Based Image Processing*, Kountchev et al., Editor 2012, Verlag Berlin Heidelberg: Springer, p. 255–314.
- [24]. Ma, Z.M., Zhang, G., Yan, L., Shape feature descriptor using modified Zernike moments. *Pattern Anal Applic.*, 2011. 14(1): p. 9–22.
- [25]. Smith, S.M., Brady, J.M., SUSAN-a new approach to low level image processing. *International Journal of Computer Vision*, 1997. 23(1): 45-78.
- [26]. Wei, C-H, Li, C-T. Content-Based Retrieval for Mammograms, In *Artificial Intelligence for Maximizing Content Based Image Retrieval*, Z. Ma, Editor 2008, Hershey (PA, USA): Idea Group Publishing, p. 313-339.
- [27]. Heikkilä, M., Pietikäinen, M., Schmid, C., Description of Interest Regions with Center Symmetric Local Binary Patterns, In *5th Indian Conference on Computer Vision, Graphics and Image Processing (ICVGIP*

- '06), P. Kalra, S. Peleg, Editor 2006, Lecture Notes in Computer Science (LNCS), volume 4338, Springer-Verlag, p.58-69.
- [28]. Digital Database for Screening Mammography
<http://marathon.csee.usf.edu/Mammography/Database.html>. Accessed 21 May 2015.
- [29]. Bahoura, M., Pattern recognition methods applied to respiratory sounds classification into normal and wheeze classes. *Computers in Biology and Medicine*, 2009. 39(9): p. 824–843.